Cold Regions Science and Technology 163 (2019) 44–58

Contents lists available at ScienceDirect

Cold Regions Science and Technology

journal homepage: www.elsevier.com/locate/coldregions

A comprehensive public-domain river ice process model and its application to a complex natural river

Julia Blackburn, Yuntong She*

Department of Civil and Environmental Engineering, University of Alberta, 7-203 Donadeo Innovation Centre for Engineering, 9211 116 Street NW, Edmonton, Alberta T6G 1H9, Canada

ARTICLE INFO

Keywords:
River hydraulics
Numerical modelling
River ice
Thermal processes
Dynamic ice
Complex natural river
River1D
Susitna River

ABSTRACT

River ice processes are challenging to study due to the risks and costs associated with data collection in harsh winter conditions. Numerical models can provide valuable insight into a river's current ice regime where data is sparse. At present, most existing one-dimensional (1D) ice process models are based on an implicit finite difference solution to the Saint-Venant equations. As a result, highly dynamic events such as rapid ice jam formation or sudden ice jam release are difficult to model due to numerical instabilities that can arise if the flow approaches supercritical. This paper presents recent developments to the University of Alberta's public-domain river ice process model, *River1D*. The model was reformulated to accommodate natural channel geometry. This new natural channel geometry version of the model was then enhanced to include water supercooling, frazil accretion, frazil re-entrainment, anchor ice formation and release, border ice formation, under-cover transport of frazil, and ice cover formation based on leading edge stability criteria. The model was applied to the Susitna River, Alaska. The model results agreed favourably with observations of water levels, flows, water temperatures, surface ice concentrations, border ice widths, ice cover progression rates, and ice thicknesses.

1. Introduction

Most northern rivers experience ice conditions for part or all of winter. River ice can significantly affect a river's regime, and in some cases, plays a larger role in flooding compared to open water conditions. The different types of river ice, and their interaction with moving river water, can affect the regime in a variety of ways. For example, as border ice grows out into the channel, the partial stationary ice cover can increase the channel resistance causing a reduction in flow under the border ice and an increase in flow in the open portion of the river (Tsang, 1970). In supercooled turbulent water, the formation of anchor ice on the river bed can affect the hydraulic resistance of the bed (Kerr et al., 2002), and its release can send waves downstream that produce measurable changes in discharge and water levels (Jasek et al., 2015). As surface ice floes travel downstream, an ice cover may be initiated if the floes come to rest due to a constriction or obstacle in the river. The ice cover progression is highly dependent on the geometry of incoming ice floes and the flow conditions at the leading edge of the ice cover (Pariset and Hausser, 1961). Incoming floes may come to rest edge to edge forming a juxtaposed ice cover when water velocities are low, or they may become unstable and entrained into the flow passing under the leading edge when water velocities are high. Entrained floes may be deposited on the underside of the downstream ice resulting in a 'hydraulically thickened' accumulation, or may be swept downstream and will not contribute to the upstream progression of the leading edge. The accumulation may collapse and thicken if its internal strength and the resistance at the banks cannot withstand the applied external forces, due to gravity and water drag. This 'mechanical thickening' will continue until a new equilibrium is achieved. As the ice front passes a location, the stage can increase dramatically and rapidly due to the sudden increase in flow resistance from the stationary ice. Once the accumulation is stable, it will freeze into an ice cover. Thickening of the ice cover can occur thermally but it can also thicken when frazil that is generated in upstream open areas is transported and deposited on the underside of the ice cover. This can also lead to the formation of hanging dams. In some cases, hanging dams can become extremely thick, reducing the flow area and increasing the under-ice velocities, which may result in bed scour (Beltaos, 2013).

These regime changes can have implications for engineering structures and aquatic ecology. Frazil ice can accumulate and block the flow to water intakes. In some severe cases, frazil ice blockage can result in collapse of the intake structure (Daly, 1991). Anchor ice can be problematic for hydropower generation. For example, anchor ice formation downstream of Manitoba Hydro's Limestone Generation Station at

* Corresponding author.
E-mail addresses: julia.blackburn@ualberta.ca (J. Blackburn), yshe@ualberta.ca (Y. She).

https://doi.org/10.1016/j.coldregions.2019.04.010
Received 12 July 2018; Received in revised form 17 April 2019; Accepted 24 April 2019
Available online 25 April 2019
0165-232X/

Sundance Rapids has caused stage increases that have resulted in millions of dollar in lost power generation revenue (Girling and Groeneveld, 1999; Malenchak, 2011). Frazil and anchor ice can also affect fish. Brown and Mackay (1995) found that cutthroat trout were excluded from overwintering pools with extensive frazil and anchor ice growth. Brown et al. (2000) reported that common carp and brown trout evacuated a pool where frazil ice had formed a hanging dam. Although freeze-up jams do not normally pose a risk to flooding since flows are typically much lower in fall and winter compared to those in spring when breakup jam occurs, they are known to pose problems to hydropower generation (Beltaos and Prowse, 2001).

River ice processes can be very challenging to study due to the risks and costs associated with data collection in remote locations, especially under harsh winter conditions. Numerical models can provide valuable insight into a river's current ice regime where data are sparse. They can also be indispensable tools for quantifying changes to the regime due to potential future conditions such as regulation and climate change. Existing models range from component models, which consider only specific ice processes, to comprehensive models, developed to simulate the entire river ice regime (Shen, 2010). Both one-dimensional (1D) and two-dimensional (2D) comprehensive river ice process models exist, commercially and within the public domain. 2D models provide a better representation of the variability of river ice processes in complex natural channel systems. However, they are not typically applied to long reaches or channel networks because costly field data and lengthy computational time render them operationally impractical. It can therefore be more practical to model real-world river ice processes over lengthy reaches using a 1D model. Most existing 1D river ice process models typically solve unsteady flow equations using implicit finite difference schemes (e.g. CRISSP1D (Shen, 2006); MIKE11-ICE (Theriault et al., 2010; Timalsina et al., 2013); and RIVICE (Lindenschmidt, 2017)) that may become unstable when the flow approaches critical or for mixed subcritical/supercritical flow situations. In order to prevent model instabilities in these cases, techniques such as the local partial inertia (LPI) technique (Fread et al., 1996) are applied to the finite difference solution to suppress the inertial terms in the Saint-Venant equations so that the solution is reduced to the more stable but less accurate diffusive wave description. These types of flow regime transitions are commonly encountered when modelling long reaches of natural rivers due to presence of rapids, waterfalls and steep canyons. For example, the Athabasca River upstream of Fort McMurray, AB, is characterized by numerous rapids that instigate dynamic breakup and a cascade of ice jam events almost yearly (Hutchison and Hicks, 2007). The upper reach of the Hay River, NWT, contains two major waterfalls and a very steep gorge section. Ice jams often occur in this section and their release ultimately result in the ice run causing peak water level and possible flooding in the Town of Hay River (Kovachis, 2011). The rapids in the Devils Canyon on the Susitna River, Alaska, periodically jam in winter but the jams typically fail and the channel remains open at these locations and they continue to produce frazil throughout winter (HDR, Alaska Inc., 2014). Furthermore, calibration and validation of the existing models were conducted towards various elements such as water levels, flows, water temperatures, ice front locations, surface ice conditions, and border ice extent, but not all of them (e.g. Timalsina et al., 2013; Theriault et al., 2010; Malenchak, 2011; Andrishak and Hicks, 2008). Without a comprehensive range of data metrics, it is difficult to correctly evaluate a given model's performance. For example, more than one combination of model parameters may create the same ice cover advancement rates, but simulated ice cover thicknesses could be drastically different for each combination of parameters.

The ultimate goal of this research is to develop a highly robust 1D comprehensive river ice process model that is capable of simulating dynamic ice processes in natural river systems with complex ice and flow regimes, and that is also available in the public domain. This paper presents new developments to the University of Alberta's public-domain river ice process model, *River1D*. The enhancements over the previous versions of the model are first described. An overview of the model's governing equations and solution procedure is then provided, followed by its application to the Susitna River in Alaska to demonstrate its new capabilities in a complex natural river system. The model results agreed favourably with observations of water levels, flows, water temperatures, surface ice concentrations, border ice widths, ice cover progression rates, as well as ice thicknesses.

2. Model description

The new river ice process model is built on the University of Alberta's public domain software *River1D*. The model was originally developed as an open water hydrodynamic model, solving the Saint-Venant equation using the characteristic-dissipative-Galerkin (CDG) finite element scheme (Hicks and Steffler, 1990, 1992). This method conserves both mass and momentum perfectly (Hicks and Steffler, 1992) and it has been proven to be consistently more stable and accurate than other schemes (finite element and implicit finite difference) particularly when modelling extreme dynamic events (Hicks and Steffler, 1992). Previous versions of the model were adapted to include several thermal (water cooling, frazil formation and rise, and ice cover formation) and dynamic (ice jam formation and release) ice processes (Andrishak and Hicks, 2005 and Andrishak and Hicks, 2008; She et al., 2009). However for these previous versions, the model application was limited to rectangular cross section geometry and site-specific ice components. In order to better simulate river ice processes in complex natural river systems, the *River1D* model was reformulated to accommodate natural channel geometry. The ice processes considered in this new natural channel geometry version of the model follow those of Andrishak and Hicks (2008) with enhancements to include water supercooling, frazil accretion, frazil re-entrainment, anchor ice formation and release, border ice formation, and under-cover transport of frazil. Additionally, ice cover formation leading edge stability criteria were implemented to simulate the ice cover progression. This accounts for the dynamic processes (i.e. hydraulic and mechanical thickening) that reduce the rate of ice cover advancement, which were modelled empirically in previous versions (Andrishak and Hicks, 2005, 2008).

2.1. Hydrodynamic equations

Accounting for the presence of a floating ice cover and anchor ice on the river bed, the conservation equation for water flow under and through the ice is:

$$\frac{\partial A}{\partial t} + \frac{\partial Q_w}{\partial x} = \frac{\rho_i}{\rho_w}\frac{\partial A_i}{\partial t} + (1 - p_a)\frac{\partial A_{an}}{\partial t} \tag{1}$$

where A is the cross sectional area to the water surface; Q_w is discharge of water under and through the ice; A_i is the cross sectional area of the surface ice including border ice and under-cover moving frazil; A_{an} is the cross sectional areas of the anchor ice; ρ_i and ρ_w are the densities of the ice and water, respectively; p_a is the porosity of the anchor ice; t represents time; and x represents the streamwise path of the river.

The momentum equation of the water flow under and through the ice is:

$$\frac{\partial Q_w}{\partial t} + \frac{\partial(\beta Q_w U_w)}{\partial x} + gA_w\frac{\partial H}{\partial x} + gA_w S_f = 0 \tag{2}$$

where U_w and A_w are the average velocity and cross sectional area of the water flowing under and through the ice, respectively; H is the water surface elevation above a specified datum; β is the momentum flux correction coefficient calculated based on Fread (1988); and S_f is the boundary friction slope. The cross sectional areas of the water and to the water surface are related through:

$$A = A_w + \frac{\rho_i}{\rho_w}A_i + (1 - p_a)A_{an} \tag{3}$$

The friction slope is evaluated using Manning's equation. When a stationary ice cover is present, the composite Manning's roughness coefficient, n_c, is calculated from the general form of the Sabaneev equation (Uzuner, 1975):

$$n_c = n_b\left(\frac{1 + \frac{P_i}{P_b}\left(\frac{n_i}{n_b}\right)^{3/2}}{1 + \frac{P_i}{P_b}}\right)^{2/3} \tag{4}$$

where n_b and n_i are the Manning's roughness coefficients for the bed and surface ice layer, respectively; and P_b and P_i are the bed-affected and ice-affected wetted perimeters of the channel, respectively. The Manning's roughness coefficient for the surface ice layer can either be user specified or it can be calculated as a function of thickness based on coefficients of Manning's roughness of the under surface of frozen slush ice obtained by Nezhikhovskiy (1964). If ice roughness is calculated, the user must specify the type of ice and roughness is interpolated based on the simulated ice thickness according to Nezhikovskiy's roughness coefficients for slush-ice cover formed principally 'from loose slush', 'from dense (frozen) slush', or 'from ice'.

2.2. Ice equations

The newly enhanced *River1D* model considers water cooling and supercooling, frazil ice formation, frazil rise and re-entrainment, border ice growth and decay, surface ice transport, thermal ice growth and decay, anchor ice evolution, under-cover transport of frazil, and ice cover progression based on leading edge stability criteria. All transport equations are solved using the Streamline Upwind Petrov-Galerkin finite element method (Brooks and Hughes, 1982). Fig. 1 illustrates the vertical ice processes considered in the model.

2.2.1. Water cooling and supercooling

Water temperature is simulated by considering the conservation of thermal energy of the water and the suspended frazil ice (ice-water mixture) following Shen (2010):

$$\frac{\partial(A_w e_{wi})}{\partial t} + \frac{\partial(Q_w e_{wi})}{\partial x} = \underbrace{-\frac{B_o(1 - C_i)}{\rho_w}\phi_{wa}}_{\text{net heat exchange between water and air}} \underbrace{-\frac{(B_o C_i + f_b B_{ws})}{\rho_w}\phi_{ia}}_{\text{net heat exchange between water and air through the ice cover air when } T_w>0°C \text{ and } T_a<0°C}$$

$$\underbrace{-\frac{(B_o C_i + P_b C_{an} + f_b B_{ws})}{\rho_w}\phi_{wi}}_{\text{net heat exchange between water and ice}} + \underbrace{B_o\frac{\rho_i}{\rho_w}L_i\eta C_f}_{\text{frazil rise when } T_w<0°C} + \underbrace{P_b C_{an}\frac{\rho_i}{\rho_w}L_i\gamma C_f}_{\text{frazil accretion to bed when } T_w<0°C}$$

$$\underbrace{-B_o C_i\frac{\rho_i}{\rho_w}L_i\beta_{re}(t_{si} + t_{fs}(1 - p_f))}_{\text{re-entrainment of surface ice to suspended frazil layer when } U_i>U_{i\_re} \text{ and } U_i>0} \underbrace{-B_o C_i\frac{\rho_i}{\rho_w}L_i\beta_{re}(t_{ui}(1 - p_f))}_{\text{re-entrainment of under-cover moving frazil to suspended frazil layer when } U_w>U_{i\_re} \text{ and } U_i=0} \tag{5}$$

where e_{wi} is the thermal energy per unit mass of the ice-water mixture ($e_{wi} = C_p(1\text{-}C_f)T_w - \rho_i C_f L_i/\rho_w$); C_p is the specific heat of water; T_w is the water temperature; C_f is the volumetric concentration of suspended frazil ice; L_i is the latent heat of ice (set to 334 KJ/kg); B_{ws} is the total width of the channel at the water surface for the main channel excluding any overbank flow; f_b is the fraction of the main channel covered by border ice; B_o is the width of the water surface not covered by border ice, $B_o = (1\text{-}f_b)B_{ws}$; C_i is the surface ice concentration; C_{an} is the fraction of the bed covered by anchor ice (user specified); ϕ_{wa}, ϕ_{ia}, ϕ_{wi} are the net rates of heat exchange per unit surface area between water and air, between water and air through the floating ice layer, and between water and ice, respectively, all quantified based on Andrishak and Hicks (2008); η is the rate of frazil rise (user specified); γ is the rate of frazil ice accretion to the bed (user specified); β_{re} is the rate of surface ice re-entrainment (user specified) that will occur when the ice velocity, U_i, is greater than the ice velocity threshold for re-entrainment, U_{i_re}; t_{si} is the thickness of the solid ice layer; t_{fs} is the thickness of the frazil slush layer; p_f is the frazil slush porosity; and t_{ui} is the thickness of the under-cover moving frazil layer. Heat exchange between the water and air uses the linear heat transfer approach to approximate the energy budget equation (Andrishak and Hicks, 2008):

$$\phi_{wa} = -\phi_s + h_{wa}(T_w - T_a) - j_{wa}T_a + k_{wa} \tag{6}$$

where ϕ_s is the net incoming solar radiation; h_{wa}, j_{wa}, k_{wa} are heat transfer coefficients; and T_a is the air temperature.

2.2.2. Suspended frazil production and transport

Once the water becomes supercooled, frazil ice will form in the water column. The concentration of suspended frazil ice changes with the thermal growth and decay of frazil ice in the water column and mass transfer between the surface ice, under-cover moving frazil, and anchor ice layers:

$$\frac{\partial(A_w C_f)}{\partial t} + \frac{\partial(Q_w C_f)}{\partial x} = \underbrace{\frac{\phi_{fw}}{\rho_i L_i}}_{\text{growth and decay}} - \underbrace{B_o\eta C_f}_{\text{frazil rise}} - \underbrace{P_b C_{an}\gamma C_f}_{\text{frazil accretion to bed}}$$

$$+ \underbrace{B_o C_i\beta_{re}(t_{si} + t_{fs}(1 - p_f))}_{\text{re-entrainment of surface ice to suspended frazil layer when } U_i>U_{i\_re} \text{ and } U_i>0} + \underbrace{B_o C_i\beta_{re}(t_{ui}(1 - p_f))}_{\text{re-entrainment of under-cover moving frazil to suspended frazil layer when } U_w>U_{i\_re} \text{ and } U_i=0} \tag{7}$$

where ϕ_{fw} is the net rate of heat exchange per unit surface area between suspended frazil particles and water and is evaluated in a similar manner to Shen et al. (1995):

$$\phi_{fw} = -\frac{2N_u^f K_w}{d_e r_o}(C_f + C_{fo})A_w T_w \tag{8}$$

where N_u^f is the Nusselt number of a suspended frazil particle; K_w is the thermal conductivity of water; d_e is the typical frazil particle thickness; r_o is the typical frazil particle radius; and C_{fo} is the frazil seeding concentration. Except for K_w, set to 0.566 W/m/°C (Shen, 2016), all parameters are user specified.

2.2.3. Border ice formation

The model simulates border ice growth from both static and dynamic processes. Static border ice is assumed to develop in the form of skim ice when the following criteria, based on Matousek (1984), are satisfied: $T_w < 0$ °C; $T_a < 0$ °C; and $U_{wl}/U_{cr} < 0.167$ where U_{wl} is the local water velocity in the open water adjacent to the edge of the border ice; and U_{cr} is the maximum water velocity for border ice accretion. The model considers lateral accretion of border ice using the following equation:

$$\frac{dB_b}{dt} = aC_i^b\left(\frac{U_{wl}}{U_{cr}}\right)^d\frac{\phi_{wa}}{\rho_i L_i} + e\frac{\phi_{DDF}}{\rho_i L_i} \tag{9}$$

where B_b is the border ice width from a given bank; ϕ_{DDF} is the rate of heat loss based on the degree days of freezing; and a, b, d, and e are user defined coefficients. The first term is based on the empirical dynamic border ice model developed by Michel et al. (1982). This term is only active when $0.167 < U_{wl}/U_{cr} < 1.0$ and $C_i > 0.1$. The second term was introduced to account for border ice growth that is not accounted by dynamic border ice formation (first term) and skim ice formation and is fashioned after the simple degree-day equation for border ice growth developed by Haresign et al. (2011). Since the first term requires the calibration of three parameters (*a, b, and d*), which may not be practical, the second term also offers the user a simpler model for

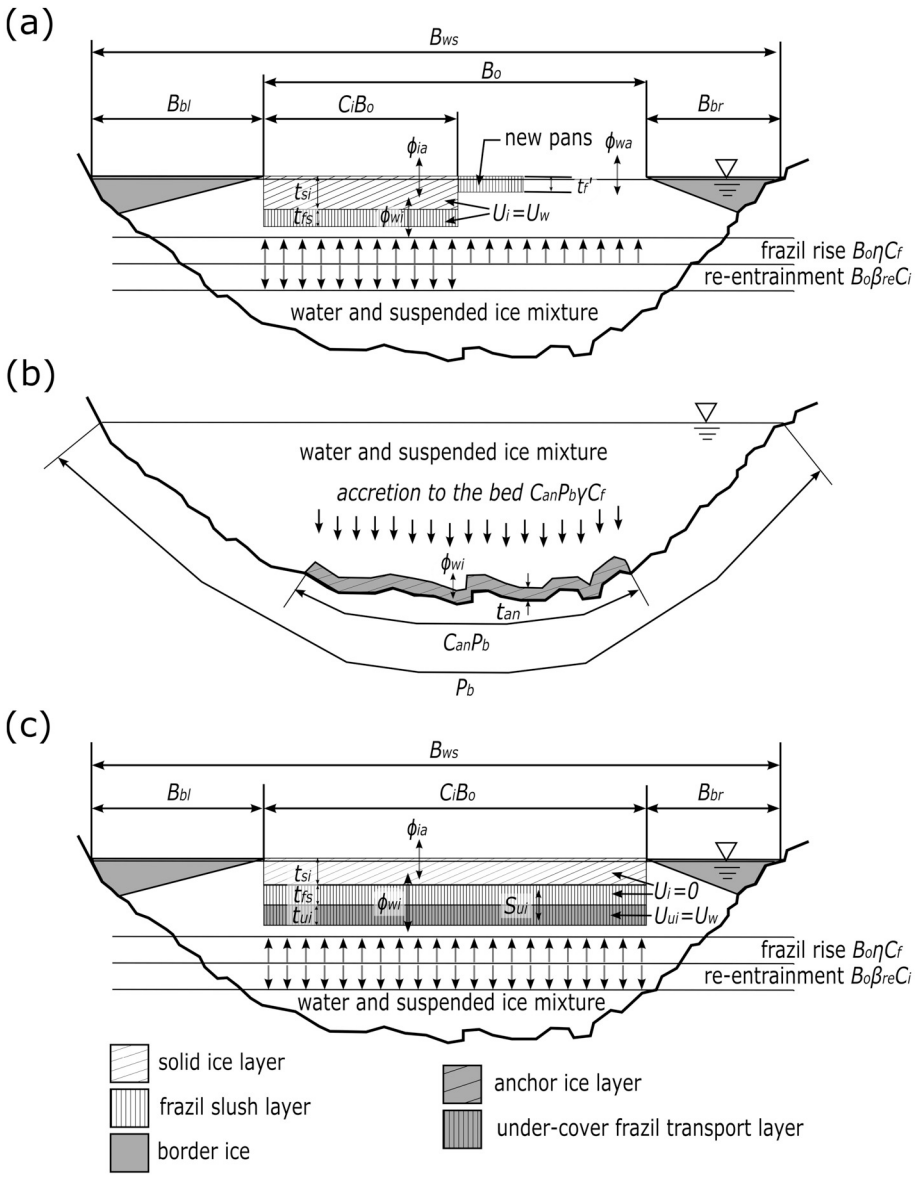

Fig. 1. Cross section definition sketch of the vertical processes considered in the model for (a) moving surface ice layers, (b) anchor ice, and (c) stationary surface ice layers with moving under-cover frazil layer adapted from Andrishak and Hicks (2008).

border ice growth that only requires the calibration of one parameter (e). Eq. (9) is evaluated at both the left (B_{bl}) and right (B_{br}) banks to obtain the total border ice width for a given cross section (B_{btotal}). The local water velocity, U_{wl}, is estimated using the following relationship:

$$U_{wl} = U_w \left(\frac{D_{wl}}{D_w} \right)^{2/3} \tag{10}$$

where D_{wl} is the local water depth at the edge of the border ice; D_w ($=A_w/T$) is the mean hydraulic depth of the water; and T is the total width of the channel.

In Clark (2013), border ice is described as "a wedge-shaped ice sheet extending from the shoreline, with the thickest portion closest to the shore and the thinnest portion actively growing laterally" as shown in Fig. 1. This description has directed the approach used to simulate the border ice thickness, t_b, and cross sectional area, A_b, in the model. The rate of growth and decay of border ice thickness, t_b, is modelled using the following equation:

$$\frac{dt_b}{dt} = \underbrace{\frac{-h_{wa}T_a - \phi_s}{\rho_i L_i \left(1 + \frac{h_{wa} t_b}{K_i}\right)}}_{\text{growth and decay}} - \underbrace{\frac{\phi_{wi}}{\rho_i L_i}}_{\text{decay}} \tag{11}$$

where K_i is the thermal conductivity of ice. The border ice thickness calculation begins once the border ice starts to grow laterally and represents the border ice thickness at each bank. It is assumed that the thickness reduces to zero at the border ice edge protruding into the channel. The average of these two thicknesses ($t_b/2$) is used to estimate the cross sectional area of the border ice:

$$A_b = \frac{B_{btotal} t_b}{2} \tag{12}$$

2.2.4. Anchor ice formation and release

The rate of change of anchor ice thickness due to frazil accretion and thermal growth and decay at a given cross section is defined by (Shen, 2010):

$$\frac{dt_{an}}{dt} = \underbrace{\frac{\gamma C_f}{(1-p_a)}}_{\text{growth due to accretion when Tw<0°C}} - \underbrace{\frac{\phi_{wi}}{\rho_i(1-p_a)L_i}}_{\text{thermal growth and decay}} \tag{13}$$

The cross sectional area occupied by the anchor ice is defined by:

$$A_{an} = C_{an}P_b t_{an} \tag{14}$$

Anchor ice release is a very important but complicated process that can occur due to mechanical and thermal processes (Malenchak, 2011). In the enhanced version of the *River1D* model, anchor ice release occurs if either the water temperature rises above zero (denoted as Condition (1)), or if the buoyancy forces of the anchor ice exceed the gravitational forces on the anchor ice (denoted as Condition (2)). Assuming tightly packed bed material based on a hexagonal close packing arrangement and negligible anchor ice growth down into the bed material pore space, Condition (2) can be expressed as:

$$t_{an} > \frac{\pi}{3\sqrt{3}} \frac{d_s(\rho_s - \rho_w)}{(1-p_a)(\rho_w - \rho_i)} \tag{15}$$

where d_s and ρ_s are the average diameter and density of the bed material, respectively (both user specified).

2.2.5. Surface ice evolution and transport

The surface ice in the model is defined by solid and frazil slush layers, assumed to travel at velocity U_i until the layers come to rest to form a stationary ice cover or accumulation. The variation in the surface ice concentration along the channel is described by:

$$\frac{\partial(B_o C_i)}{\partial t} + \frac{\partial(U_i B_o C_i)}{\partial x} = \underbrace{\frac{B_o(1-C_i)\eta C_f}{t'_f(1-p_f)}}_{\text{frazil rise}} + \underbrace{\frac{B_o(1-C_i)\phi_{wa}}{t'_{si}\rho_i L_i}}_{\text{freezing between ice pans once ice has stopped when } U_i=0 \text{ and } T_a<0} + \underbrace{\frac{(1-C_i)S_{ui}}{(1-p_f)t_{ui}}}_{\text{transfer from under-cover moving frazil layer}} - \underbrace{B_o\beta_{re}C_i}_{\text{re-entrainment of surface ice when } U_i>U_{i\_re}} \tag{16}$$

Where t'_f is the thickness of new frazil pans; t'_{si} is initial thickness of newly formed solid ice between the ice pans once the ice has stopped moving; and S_{ui} is a source term representing the exchange between the under-cover moving (A_{ui}) and stationary (A_{fs}) frazil layers.

The conservation of mass equation for the frazil slush layer is described by:

$$\frac{\partial A_{fs}}{\partial t} + \frac{\partial U_i A_{fs}}{\partial x} = \underbrace{\frac{B_o\eta C_f}{(1-p_f)}}_{\text{frazil rise when } U_i>0} - \underbrace{\frac{B_o C_i \phi_{ia}}{\rho_w p_f L_i}}_{\text{pore water freezing when } A_{fs}>0 \text{ and } T_a<T_w\le 0°C} - \underbrace{\frac{B_o C_i \phi_{wi}}{\rho_i(1-p_f)L_i}}_{\text{decay at water-ice interface when } A_{fs}>0 \text{ and } T_w>0°C} - \underbrace{B_o C_i \beta_{re} t_{fs}}_{\text{re-entrainment of surface ice when } U_i>U_{i\_re} \text{ and when } U_i>0} + \underbrace{\frac{S_{ui}}{(1-p_f)}}_{\text{transfer from under-cover moving frazil layer}} \tag{17}$$

where A_{fs} is the cross sectional area of the frazil slush layer ($A_{fs} = B_o C_i t_{fs}$).

For the solid ice layer, the mass conservation equation is expressed as:

$$\frac{\partial A_{si}}{\partial t} + \frac{\partial U_i A_{si}}{\partial x} = \underbrace{f_1 \frac{B_o C_i \phi_{ia}}{\rho_i L_i}}_{\text{growth and decay}} - \underbrace{\frac{B_o C_i \phi_{wi}}{\rho_i L_i}}_{\text{growth and decay at water-ice interface when } A_{fs}=0} + \underbrace{\frac{B_o(1-C_i)\phi_{wa}}{\rho_i L_i}}_{\text{freezing between ice pans once ice has stopped when } U_i=0 \text{ and } T_a<0} - \underbrace{B_o C_i \beta_{re} t_{si}}_{\text{re-entrainment of surface ice when } U_i>U_{i\_re} \text{ and when } U_i>0} \tag{18}$$

where A_{si} is the cross sectional area of the solid ice layer ($A_{si} = B_o C_i t_{si}$) and f_1 is a conditional constant that is defined as follows.

$$f_1 = \begin{cases} 1 & \text{when } \phi_{ia} < 0,\ A_{si} > 0, \text{ and } T_a > 0°C \text{ (melting of solid ice)} \\ 1 & \text{when } \phi_{ia} > 0,\ A_{fs} = 0, \text{ and } T_w \le 0°C \text{ (freezing of water column)} \\ \rho_i(1-p_f)/\rho_w p_f + 1 & \text{when } \phi_{ia} > 0,\ A_{fs} > 0 \text{ and } T_w \le 0°C \text{ (freezing of pore water)} \\ 0 & \text{otherwise} \end{cases} \tag{19}$$

The border ice, under-cover moving frazil ice, and surface ice are related through:

$$A_i = A_{si} + (1-p_f)(A_{fs} + A_{ui}) + A_b \tag{20}$$

2.2.6. Ice cover progression

Ice cover formation is assumed to occur based on a single bridging location that is user specified. Once bridging occurs, incoming ice will accumulate to form a stationary ice cover in the upstream direction either by floe juxtaposition, hydraulic thickening, or mechanical thickening based on the Froude number immediately upstream of the leading edge, F_r, defined as $U_w/\sqrt{gD}$. The ice front location, X_i, is tracked using the following equation (Uzuner and Kennedy, 1976):

$$X_i^{t+\Delta t} = X_i^t - \frac{C_i(t_{si} + (1-p_f)t_{fs})U_i \Delta t}{t_{le}(1-p_j) - C_i(t_{si} + (1-p_f)t_{fs})} \tag{21}$$

where t and $t + \Delta t$ are the model times corresponding to the ice front location; Δt is the simulation time step; t_{le} and p_j are the thickness and porosity of the ice accumulation, respectively, that are expected once the ice cover forms. The location of the ice front, also called the leading edge, is used to specify the velocity of the ice in the model, as shown in Fig. 2.

Upstream of the leading edge, the surface ice (frazil slush and solid ice layers) is assumed to travel at the speed of the water ($U_i = U_w$). Downstream of the leading edge, the surface ice is assumed to be stationary ($U_i = 0$) and the under-cover frazil transport layer is assumed to travel at the speed of the water ($U_{ui} = U_w$). Estimates for t_{le} are dependent on the ice cover progression mode as described in Shen (2016). Specifically, when F_r is less than the user specified maximum Froude number for juxtaposition, F_{r_jux}, the ice cover progresses upstream in juxtaposed mode, and the value of t_{le} is set to the thickness of the incoming ice floes ($t_{si} + t_{fs}$). Whereas, when the Froude number is between F_{r_jux} and the maximum Froude number for ice cover advancement, F_{r_max}, the ice cover will progress upstream in either hydraulic thickening or mechanical thickening mode. Values of t_{le} are calculated using narrow ice jam and equilibrium ice jam theory (Pariset and Hausser, 1961; Pariset et al., 1966); the governing theory is determined by the one that produces the larger value of t_{le}. The equilibrium ice jam equation requires values be input for μ, a composite jam stress parameter (involving internal friction properties and porosity of the ice accumulation), and τ_c, the ice cohesion. The porosity of the ice accumulation is estimated using (Shen, 2016):

$$p_j = p_c + (1-p_c)\left(\frac{p_f t_{fs}}{t_{si} + t_{fs}}\right) \tag{22}$$

where p_c represents the space between the ice floes in the newly formed ice cover.

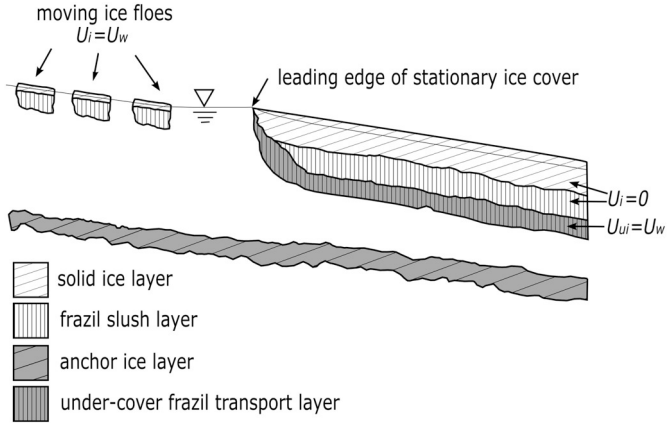

Fig. 2. Longitudinal profile definition sketch showing the modelled ice layers.

In the model, the surface ice and under-cover transport layers are confined to the width of the channel between the border ice. Since frazil does not accumulate below the border ice, the flow may never stage up to the level that it would in nature to allow the Froude number to drop below F_{r_max} and simulated ice cover advance rates may be slowed or stalled compared to observed rates.

2.2.7. Under-cover transport of frazil

Transport of frazil along the underside of the stationary ice cover is defined by:

$$\frac{\partial A_{ui}}{\partial t} + \frac{\partial U_{ui} A_{ui}}{\partial x} = \underbrace{\frac{B_o \eta C_f}{(1 - p_f)}}_{\substack{\text{frazil rise} \\ \text{when } U_i = 0}} - \underbrace{B_o C_i \beta_{re} t_{ui}}_{\substack{\text{re-entrainment} \\ \text{of under-cover moving} \\ \text{frazil when } U_{ui} > U_{i\_re} \\ \text{and when } U_i = 0}} - \underbrace{\frac{S_{ui}}{(1 - p_f)}}_{\substack{\text{transfer to} \\ \text{frazil slush} \\ \text{layer}}} \tag{23}$$

where A_{ui} is the cross sectional area of the under-cover moving frazil layer ($A_{ui} = B_o C_i t_{ui}$); and U_{ui} is the velocity of this layer. In discrete form, the source term is evaluated as follows:

$$S_{ui} = \frac{Q_{uit} - Q_{uic}}{L} \tag{24}$$

where L is the length of the ice cover between computational nodes (approximated in the model by the streamwise discretization); Q_{uit} is the total under-cover ice discharge ($A_{ui}U_{ui}(1\text{-}p_f) + A_w C_f U_w$); and Q_{uic} is the ice transport capacity which follows Shen and Wang (1995):

$$Q_{uic} = 5.487 F d_f B_o \sqrt{g d_f \left(\frac{\rho_w - \rho_i}{\rho_w}\right)} (\Theta - \Theta_c)^{1.5} \text{where} \, \Theta \geq \Theta_c \tag{25}$$

and the dimensionless flow strength,Θ, is:

$$\Theta = \frac{\tau_i}{F^2 g d_f (\rho_w - \rho_i)} \tag{26}$$

where τ_i is the shear stress on the underside of the stationary frazil slush and solid ice layers; F is the frazil particle shape factor; and d_f is the average diameter of frazil granules in under-cover transport layer. When Θ is less than the critical flow strength, Θ_c, there is no under-cover frazil transport ($Q_{uic} = 0$).

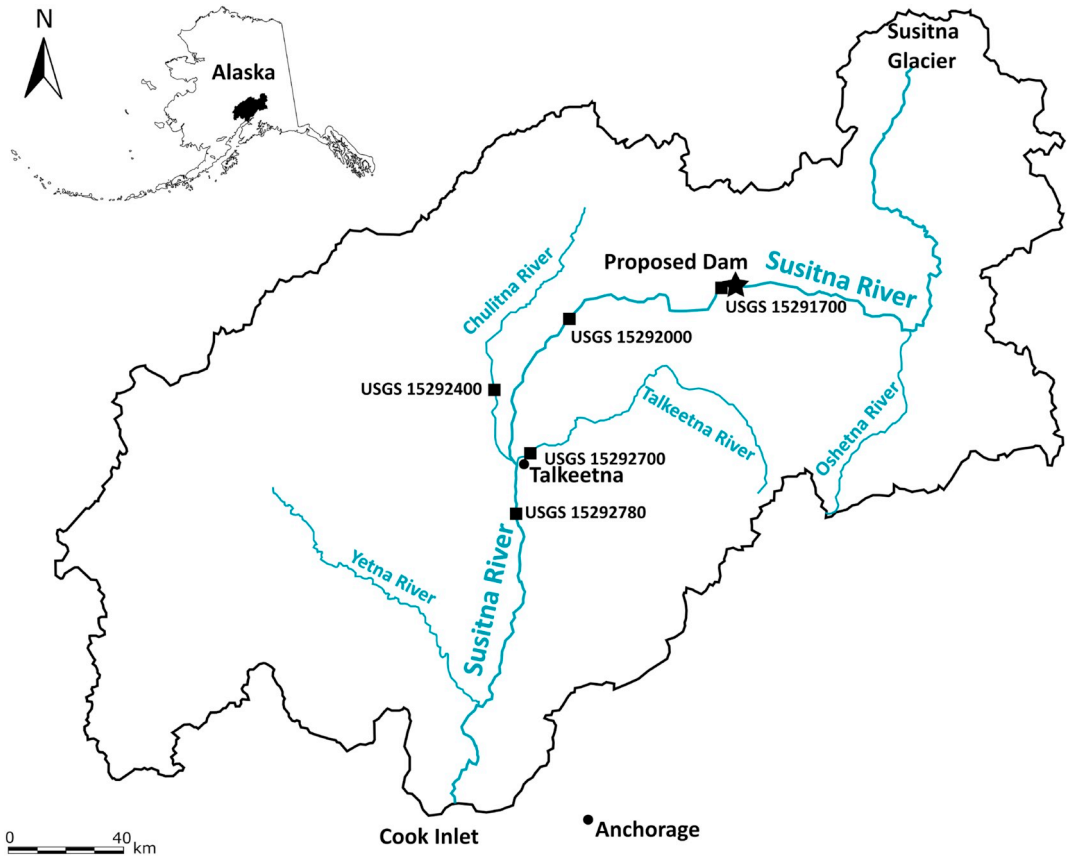

Fig. 3. The Susitna River basin.

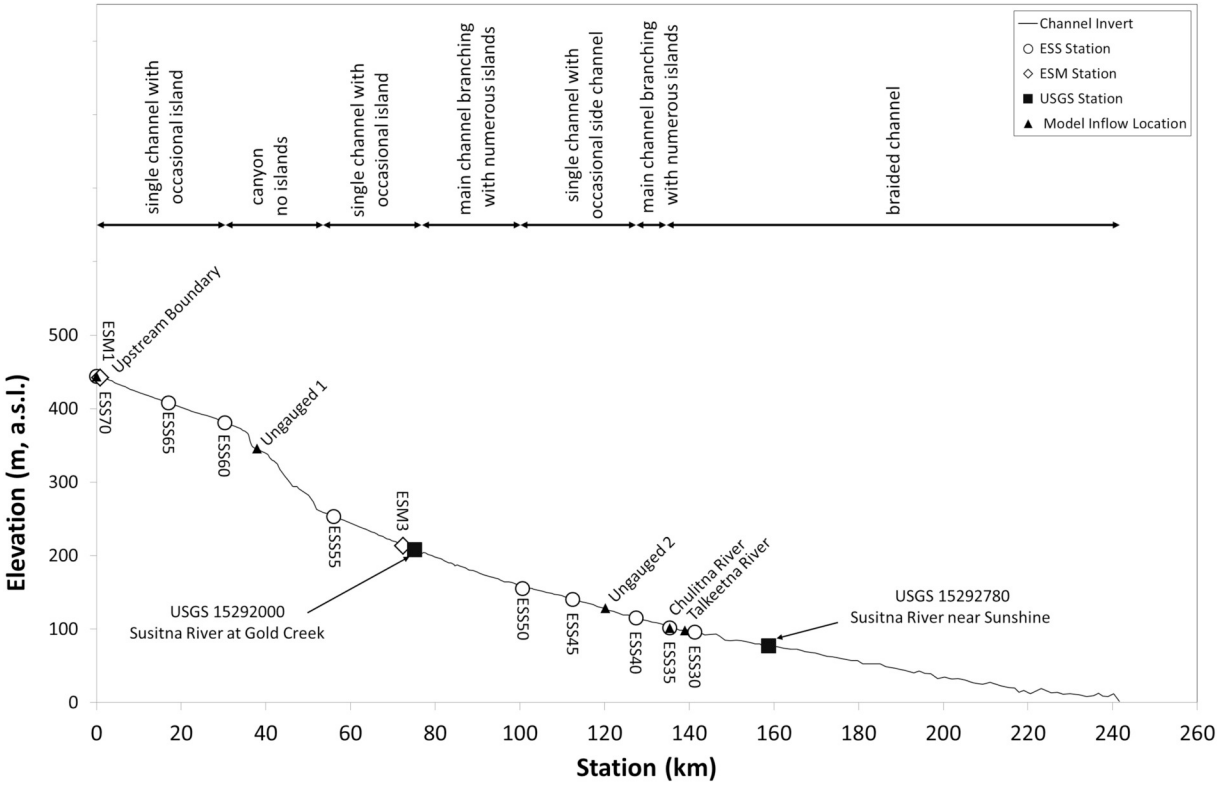

Fig. 4. Susitna River profile showing channel invert, sub reach descriptions, USGS and ESS station locations, and model inflow locations.

3. Model application

3.1. Study site and available data

The newly enhanced *River1D* ice process model was applied to the Susitna River, located in south-central Alaska. The Susitna River, shown in Fig. 3, stretches 504 km from its headwaters at the Susitna Glacier, in the Alaska Range to the Cook Inlet in the Gulf of Alaska with a drainage area of 51,800 km^2 and an average discharge at the mouth of 1444 m^3/s (Kammerer, 1990). The model study reach extends from the location of the proposed Susitna-Watana Dam site down to the confluence with the Yetna River, a length of approximately 241 km. The study reach was categorized into seven subreaches based on channel geomorphology (e.g. planform pattern, channel slope, and roughness features) as shown in Fig. 4. Stationing is measured starting from the model upstream boundary at the location of the proposed dam.

All data for this modelling study were made available by HDR Alaska, Inc. (HDR) as part of the Alaska Energy Authority's (AEA) license application for the Susitna-Watana Hydroelectric Project (Project). For the Project, a total of 246 cross sections were surveyed along the study reach. Cross sections were interpolated with a maximum spacing between sections of 322 m for a total of 875 modelled cross sections.

Inflows to the study reach were provided at five locations along the study reach: one inflow boundary and four lateral inflow boundaries (Fig. 4). Two of the lateral inflows were provided to account for ungauged tributaries entering the study reach (Ungauged 1 and Ungauged 2) while the other two were to account for the inflows from the Chulitna and Talkeetna Rivers. Gauge data (water levels and flows) at Susitna River at Gold Creek (USGS 15292000) and Susitna River near Sunshine (USGS 15292780) were provided for comparison with model results. Continuous water level, water temperature, and air temperature data were available at nine Project stations along the study reach, labelled with the prefix ESS (Alaska Energy Authority station on the Susitna River for Surface water). Water temperatures at the five inflow boundaries were provided by HDR and were also available at USGS 15292780 for comparison with model results. Net incoming solar radiation data were available at two ESM (Environmental Susitna Monitoring) stations: ESM1 and ESM3. However, due to potential data quality and orographic effects at ESM3, only the data from ESM1 was used in the modelling. USGS, ESS, and ESM station locations are shown in Fig. 4. Air temperature data at the ESS stations were applied to each cross section in the model based on the nearest station to the cross section. The net solar radiation from ESM1 was applied to all cross sections. Ice data for model freeze-up calibration and validation included incoming surface frazil at the upstream boundary (estimated from hourly photos taken at ESS70); ice cover progression from the time of bridging onward; and winter ice thickness, water level and discharge data at a few selected cross sections. The data also included observations of surface ice concentration, border ice widths, and anchor ice areal coverage, all obtained from aerial photos, aerial video, or from remote cameras installed at a number of the ESS stations. No water level data were available at the downstream boundary. For this reason a constant water level was assumed at this boundary for both open water and ice covered conditions. A value of 13.7 m was selected to ensure minimal backwater effects based on a sensitivity analysis (13.7 ± 1.5 m only affects the water levels within the last 19 km of the model domain which is more than 64 km downstream of the most downstream gauge, USGS 15292780, used in the model calibration and validation).

3.2. Open water calibration and validation

The model was calibrated and validated for six open water events in 2012 and 2013. Model calibration was completed by adjusting the main channel roughness values within each of the seven subreaches. Calibrated Manning's roughness values range from 0.025 in the braided reach to 0.050 in the canyon (known as the Devils Canyon). Floodplain roughness values were set based on engineering judgement by HDR with a value of 0.15 at most cross sections. For open water, a calibration

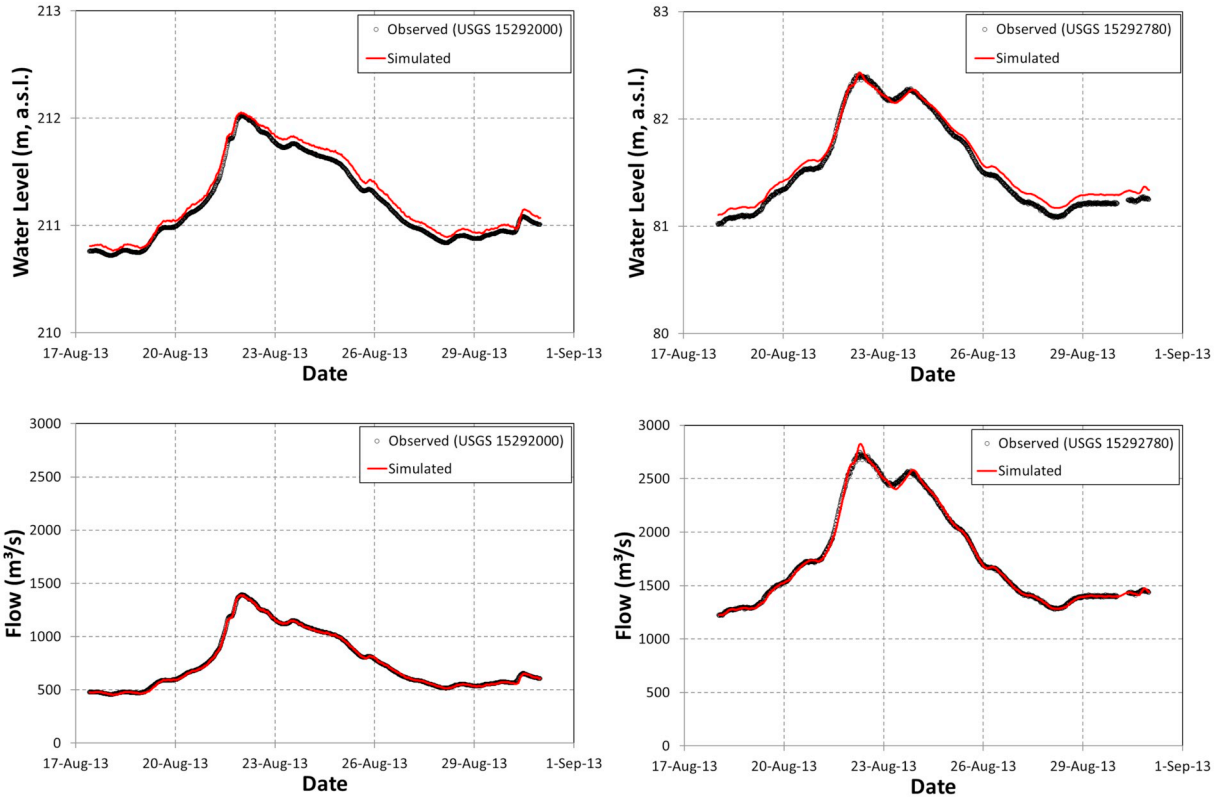

Fig. 5. Simulated and observed water levels and flows at USGS 15292000 and USGS 15292780.

tolerance of 0.3048 m (1 ft) was selected by taking into account the magnitude of potential errors in measuring water levels on a river of this size and type (e.g. wave effects, instrument error, and survey error) as well as two dimensional effects (such as flow super-elevation).

At the two USGS stations, the model results showed good agreement with the observed flows with a Nash-Sutcliffe model efficiency (Nash and Sutcliffe, 1970) of no less than 0.96 for all events. For the events, the mean absolute errors in the water levels are less or equal to the 0.3048 m tolerance at all stations except at ESS35 where it is above this tolerance for one event (0.46 m). Since this station is immediately downstream of the confluence with the Chulitna River, where the flow is likely very two-dimensional in nature, the model is not expected to perform particularly well at this location. Fig. 5 shows simulated and observed results at the USGS stations for one of the events. Water levels are reported in metres above sea level (m, a.s.l.).

3.3. Freeze-up calibration and validation

Data collected during the 2012–2013 freeze-up period were used for model calibration; the 2013–2014 data set was used for model validation. Calibration of the model ice parameters was performed in steps. The first step was to calibrate the parameters that control the water temperature. These parameters include the heat transfer coefficients in the heat exchange between the water and air, ϕ_{wa} (Eq. (6)). For the heat transfer coefficient, h_{wa}, a value of 20 W/m^2/°C was found to be the most appropriate. Fig. 6 provides a comparison between the modelled and observed water temperature at ESS50 and USGS 15292780 for the calibration period. The same stations are compared for the validation period in Fig. 7. Although the linear heat transfer model has additional parameters (i.e. j_{wa}, k_{wa}), they were set to zero as it was found that the modelled temperature corresponded well to the observed using only h_{wa} and the net incoming solar radiation, ϕ_s. For both the calibration and validation period, the model was able to simulate both the variation in the water temperature through the cool down period and also the point in time when the water reached (and generally stayed at) zero degrees, demarking the start of the freeze-up. The differences between the simulated and observed values at USGS 15292780 that occur after October but before the water drops to zero may be the results of assumptions that were made in order to fill gaps in the data needed for model inputs. Because water temperature data were not available for the Chulitna and Talkeetna Rivers, input values at these two inflow boundaries were assumed to be equal to the water temperatures at ESS35. Additionally, input air temperature data collected at ESS30 were used to represent the air temperatures for the last 100 km of the domain. Lastly, net incoming solar radiation was only available at the upstream end of the domain at ESM1 which is approximately 100 km away from USGS 15292780. Because of the orographic effect of the mountainous terrain, the differences between the assumed and actual values for any of these model inputs could be significant and negatively impact the simulated water temperatures.

The next step was to calibrate the ice modelling parameters that relate to the river ice but prior to the formation of a stationary ice cover (e.g. frazil, anchor and border ice). Where available, collected data were used to directly set parameters; otherwise, the values were adjusted so that simulated values best matched observed ones using the range of values found in the literature as guidance. Table 1 summarizes the adopted values for the ice modelling parameters for the freeze-up simulations.

In order to properly calibrate the frazil formation component of the model, data quantifying the amount of frazil in the river is needed. Since only areal ice coverages were collected during freeze-up (no thicknesses), it was difficult to calibrate the ice production in the model. For this reason, the frazil production parameters (C_{fo}, d_e, r_o, N_u^f) were taken from values in the literature (see Table 1). The thickness of newly formed ice pans, t_f', was set based on the average thickness of incoming frazil at the upstream boundary during the 2012 freeze-up period, 0.2 m. The rate of frazil rise, η, was adjusted so that modelled surface ice concentrations matched reasonably well with the observed.

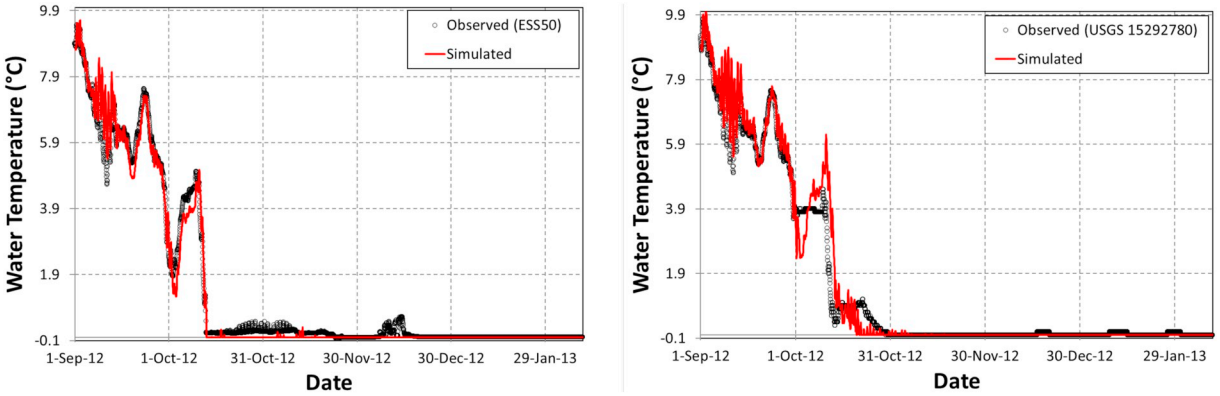

Fig. 6. Simulated and observed water temperatures at ESS50 and USGS 15292780 for the 2012–2013 calibration period.

Fig. 8 shows a comparison of observed surface ice concentrations with simulated values for late November for both the calibration (2012) and validation (2013) events. Although there is significant variability between the observed and simulated ice concentrations, the simulated values are generally similar to the observed ones in terms of magnitude. The average simulated surface ice concentration on November 28th, 2012 for the first 95 km of the domain (upstream of the simulated ice front) is 37%, while the observed average for the same reach on that day is 40%. Similarly, the average simulate surface ice concentration on November 29th, 2013 is 40% upstream of the simulated ice front (first 109 km) and the observed average is 66%. The validation data do not agree as well; however, there were fewer data points to calculate the average for 2013 compared to 2012. Additionally, variability between the observed and simulated concentrations may be due in part to model results being output at a specific point in time whereas the observed ice concentrations were recorded at various times through the day.

It was noticed that the model underestimated the border ice widths when only the skim and dynamic border ice components were simulated and parameters in the dynamic component (i.e. a, b, d, and U_{cr}) were set based on the values in Michel et al. (1982). Rather than adjusting the parameters in the dynamic border ice component of the border ice model, in order to simulate the widths that were in better agreement with the observed ones, the parameter e was adjusted until the simulated and observed values matched reasonably well. The maximum fraction of the channel that can be occupied by border ice, f_{bmax}, was set to 0.7. This was set to prevent the channel from completely closing at any section upstream of the ice front, since the model can presently only accommodate bridging at a single location. Fig. 9 shows simulated and observed total border ice widths in early December for both the calibration and validation events. For the calibration event, where border ice widths were reported at most cross sections upstream of Talkeetna (km 139), the model did quite a good job of capturing the variability in the data. For example, the observed and simulated values are both generally around or below 50 m in the reach between km 35 and km 52. Unfortunately, the same level of detail was not available for the validation border ice data but the reported values do show the same trend of around 50 m or less compared to the simulated values for the same reach.

Data for the anchor ice component included areal coverages and bed material sizes. The fraction of the channel that gets covered by anchor ice in the model, C_{an}, was calculated based on anchor ice widths observed during the 2012 freeze-up period. These widths were converted to a percent coverage and the average was taken. The percent coverage values collected in the first 140 km of the domain between October and December 2012 are presented in Fig. 10. The figure illustrates the significant presence of anchor ice in the river during the freeze-up process and the need to include this process in the model. The bed material average diameter, d_s, in the anchor ice release model, was set to 0.05 m based on the weighted average of bed material sizes reported in Tetra Tech, Ice (2013). Since anchor ice thicknesses were not available to calibrate the anchor ice accretion rate, γ, and the anchor ice porosity, p_a, these parameters were set based on the values in the literature.

The last step was to calibrate the model's ability to simulate the ice cover progression during freeze-up. Time of bridging at the downstream boundary and ice front location data were provided for the calibration and validation events. The ice cover was observed to bridge at other locations along the domain but a general ice front progression was interpreted from the data (by neglecting open leads and intermediary bridging locations) for comparison with the simulated ice front progression. The maximum Froude number for juxtaposition, F_{r_jux}, was set to 0.06 based on Lal and Shen (1991). However, the ice cover progression was not found to be sensitive to this parameter indicating that the ice cover generally progressed in either hydraulic thickening or

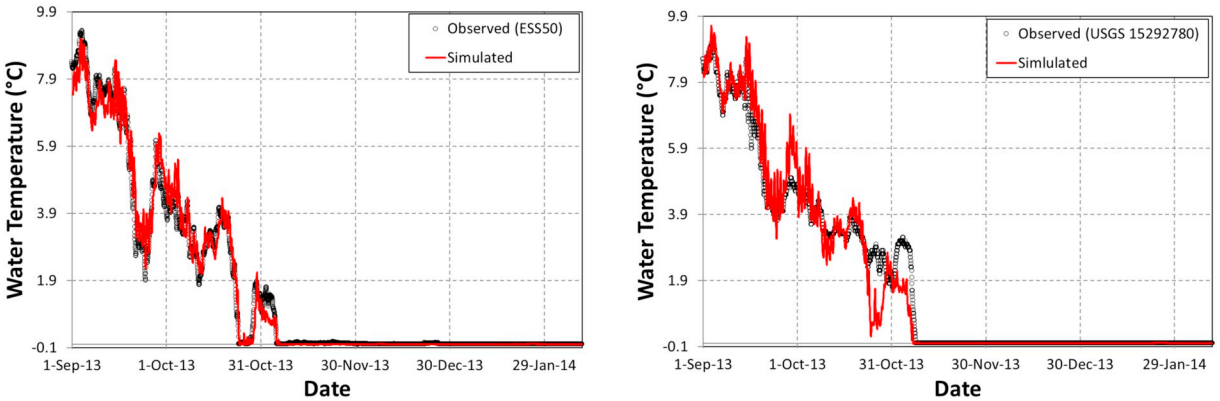

Fig. 7. Simulated and observed water temperatures at ESS50 and USGS 15292780 for the 2013–2014 validation period.

Table 1
Adopted values for ice modelling parameters.

Ice modelling parameter	Adopted value	Values in literature
Density of ice, ρ_i (kg/m^3)	917	Lal and Shen (1991)
Heat transfer coefficient, h_{wa} (W/m^2/°C)	20	19.7 (Lal and Shen, 1991) 15 (Andrishak and Hicks, 2008) 20 (Timalsina et al., 2013; Calkins, 1984)
Frazil seeding concentration, C_{fo}	0.00001	
Typical frazil particle thickness, d_e (m)	0.0003	0.0003 (Wang et al., 1995) 0.00013 (Malenchak, 2011)
Typical frazil particle radius, r_o (m)	0.001	0.001 (Wang et al., 1995; Malenchak, 2011)
Nusselt number for typical suspended frazil particle, N_u^f	4.0	4.0 (Wang et al., 1995; Malenchak, 2011)
Coefficient of turbulent heat exchange, α_{wi} (Ws$^{0.8}$/m$^{2.6}$/°C)	1187	1187 (Ashton, 1973; Andrishak and Hicks, 2008)
Rate of frazil rise, η (m/s)	0.0005	0.001 (Wang et al., 1995) 0.0001 (Andrishak and Hicks, 2008) 0.0004 (Jasek et al., 2011) 0.00009 (Timalsina et al., 2013)
rate of surface ice re-entrainment, β_{re} (1/s)	0.00001	0.00001 (Wang et al., 1995; Malenchak, 2011)
Re-entrainment velocity threshold, U_{i_re} (m/s)	1.06	
Porosity of frazil slush layer, p_f	0.4	0.5 (Andrishak and Hicks, 2008) 0.4 (Lal and Shen, 1991)
New frazil pan thickness, t'_f (m)	0.2	0.3 (Andrishak and Hicks, 2008) 0.2 (Timalsina et al., 2013)
Solid ice initial thickness, t'_{si} (m)	0.001	0.001 (Lal and Shen, 1991)
Frazil particle shape factor, F	1.0	1.00 ± 0.03 (Beltaos, 2013) 1.0 (Shen and Wang, 1995)
Average diameter of frazil granules in coverload, d_f (m)	0.01	0.01 (Shen and Wang, 1995)
Critical flow strength for under-cover frazil transport, Θ_c	0.041	0.041 (Shen and Wang, 1995)
Porosity of anchor ice, p_a	0.4	0.4 (Malenchak, 2011)
Frazil accretion rate, γ(m/s)	0.00001	0.000001 (Wang et al., 1995) 0.000005–0.00025 (Malenchak, 2011) 0.0001 (Timalsina et al., 2013)
Fraction of bed covered by anchor ice, C_{an}	0.25	
Bed material average diameter, d_s (m)	0.05	
Bed material density, ρ_s (kg/m^3)	2650	2650 (Malenchak, 2011)
Border ice equation coefficient, a	14.1	14.1 (Michel et al., 1982)
Border ice equation coefficient, b	1.08	1.08 (Michel et al., 1982)
Border ice equation coefficient, d	−0.93	−0.93 (Michel et al., 1982)
Border ice equation coefficient, e	9.75	
Maximum fraction of channel covered by border ice, f_{bmax}	0.7	
Maximum velocity for dynamic border ice growth, U_{cr} (m/s)	1.2	1.2 (Michel et al., 1982)
Maximum Froude number for juxtaposition, F_{r_jux}	0.06	0.06 (Lal and Shen, 1991)
Maximum Froude number for ice cover progression, F_{r_max}	0.097, 0.15	0.08 to 0.13 (Ashton, 1986) 0.09 (Lal and Shen, 1991) 0.094 (Calkins, 1984) 0.08 (Timalsina et al., 2013)
Space between ice floes in newly formed cover, p_c	0.4	Shen (2016)
Composite jam stress parameter, μ	1.28	1.28 (Pariset and Hausser, 1961; Pariset et al., 1966; Lal and Shen, 1991)
Ice cohesion, τ_c (Pa)	700	700 (Calkins, 1984) 980 (Lal and Shen, 1991)

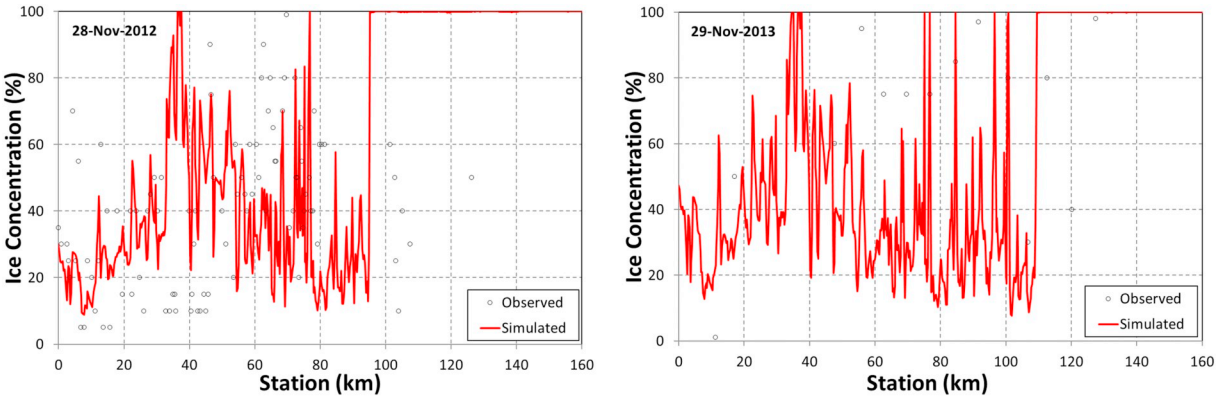

Fig. 8. Simulated and observed surface ice concentrations in late November for the calibration and validation events.

mechanical thickening mode. Two values of F_{r_max} were used to simulate the ice cover progression. For most of the domain F_{r_max} = 0.097 best fit the general progression; however, a value of F_{r_max} = 0.15 was required in the braided reach downstream of USGS 15292780, which is outside of the range of expected values for this parameter (Table 1). A possible reason for this is that the one-dimensional modelling approach is not able to accurately simulate the flow properties in the braided reach where the flow is expected to be more two-dimensional in nature.

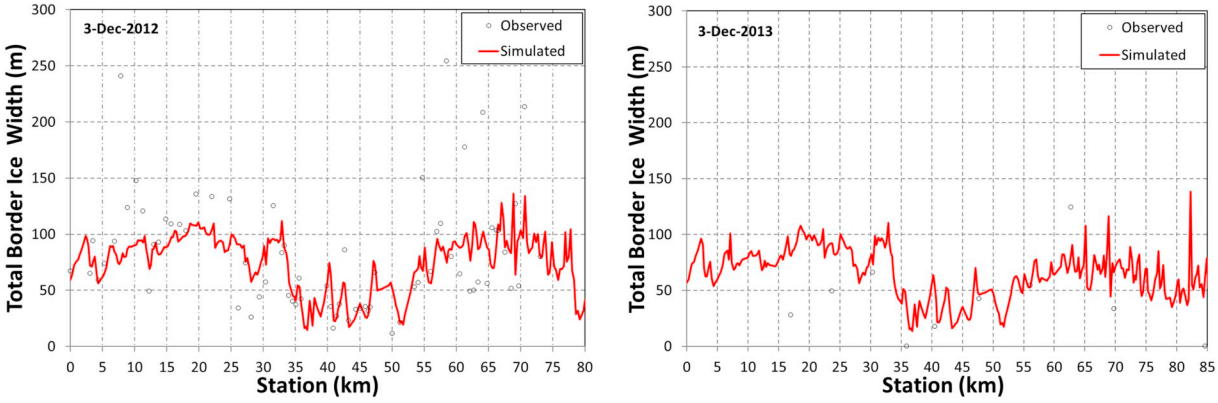

Fig. 9. Simulated and observed border ice widths early December for the calibration and validation events.

The composite jam stress parameter, μ, was set to 1.28, based on values in the literature (see Table 1) and the ice cohesion, τ_c, was set to 700 Pa as this value was used in a previous ice model of the Susitna River (Calkins, 1984). The simulated ice cover progressions are compared to the interpreted general ice front locations in Fig. 11 for both the calibration and validation events.

Overall the model is capable of capturing the general progression of the ice front up to the downstream end of the canyon (km 53). However, the data show that the ice cover does initiate at multiple bridging locations which cannot be simulated by the current version of the model. This limitation is something that should be addressed in the future to allow for more accurate simulation of an ice cover with multiple ice fronts. The simulated ice cover progression stalls in the canyon (km 30 to km 53) which is consistent with freeze-up observations that the channel remains mostly open through the canyon throughout winter (HDR, Alaska Inc., 2014). But because the model does not currently consider stability of the ice cover once the ice cover has formed, the model is not able to simulate the retreat of the ice front due to jam failure in the canyon as reported by HDR, Alaska Inc. (2014). Therefore, future model developments should also include a means of evaluating ice cover stability to determine whether the ice cover may collapse and cause retreat of the ice front.

Water level data, available at a number of USGS and ESS stations, were used to calibrate and validate the ice roughness parameter in the

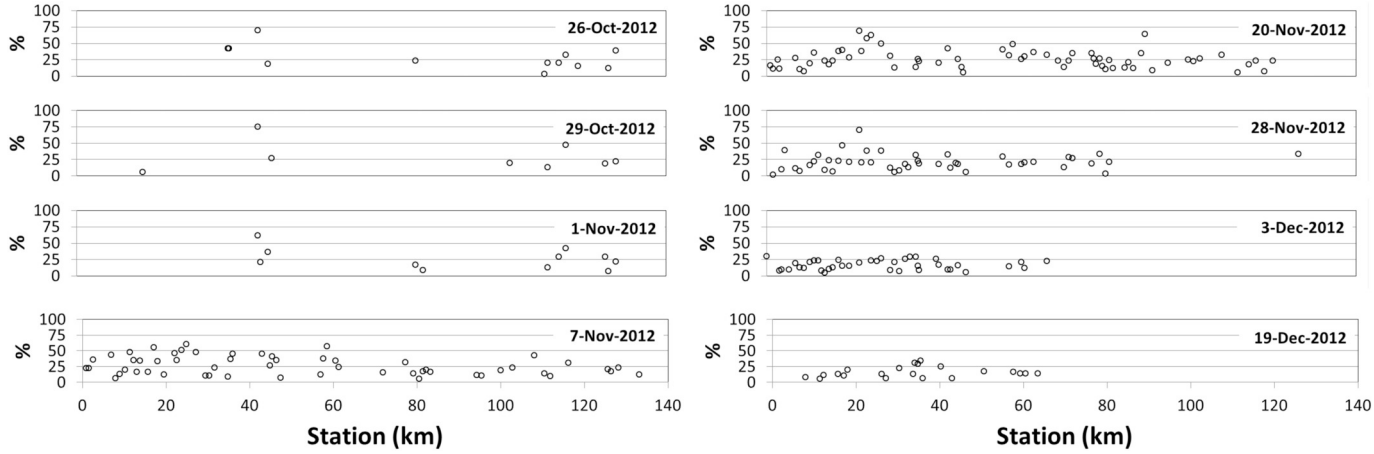

Fig. 10. Observed percent coverage of anchor ice along the domain on various days through the 2012 freeze-up period.

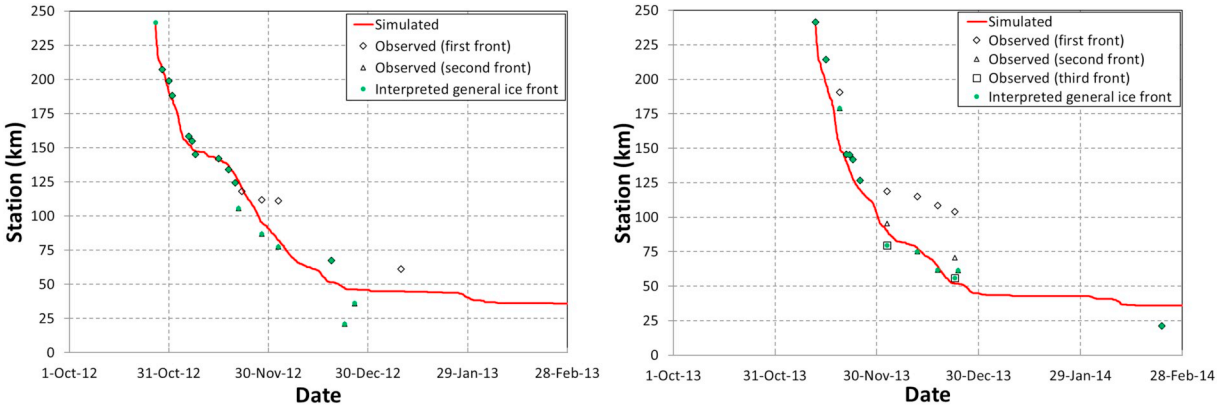

Fig. 11. Simulated and observed ice front progression for the calibration and validation events.

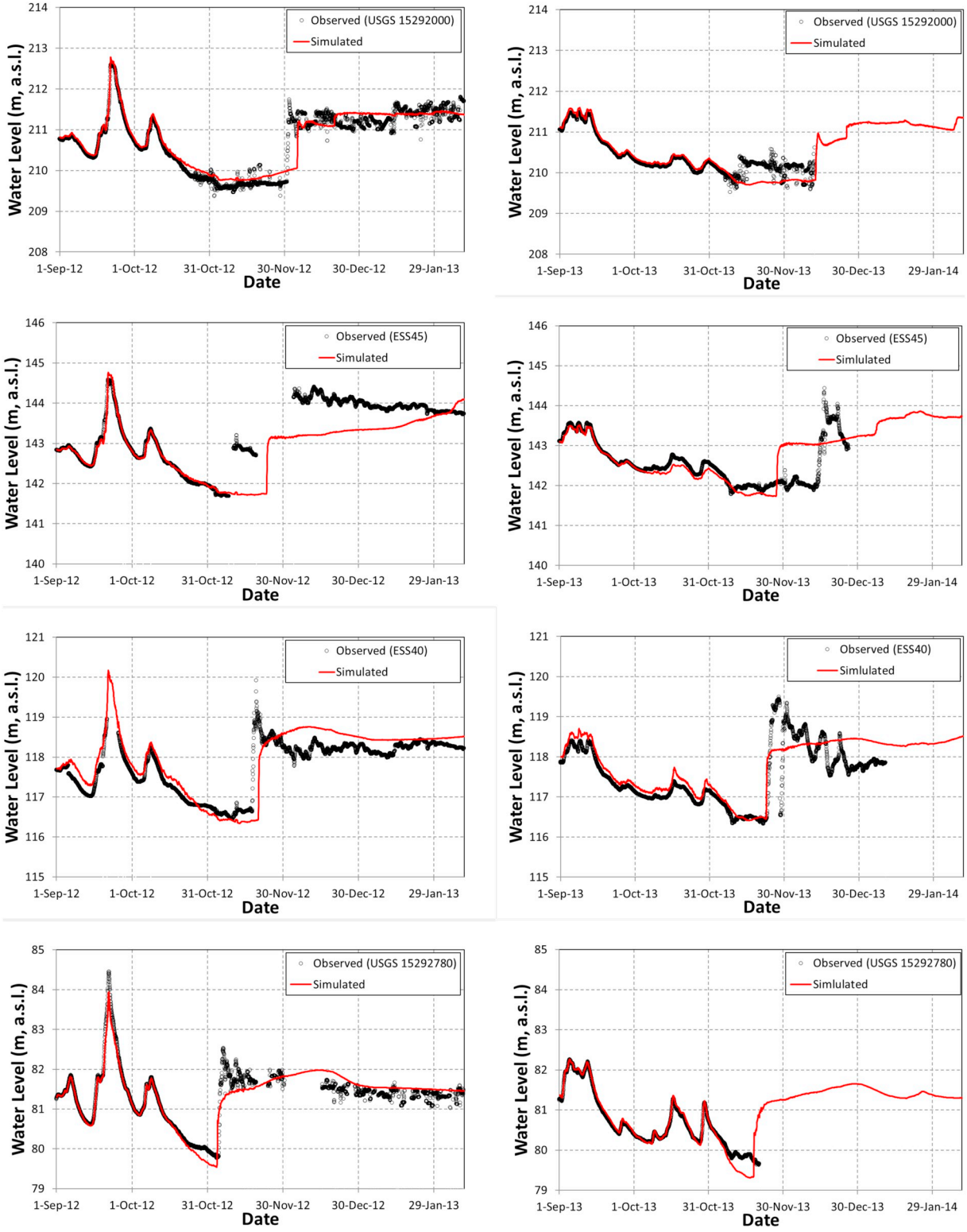

Fig. 12. Simulated and observed water levels at USGS 15292000, ESS45, ESS40, and USGS 15292780 for the calibration and validation events.

model. Ice roughness values were interpolated based on ice thickness using the 'from ice' option. Simulated water levels are compared to observed levels in Fig. 12 at four of the stations that were operational for both the calibration and validation events. Unfortunately the gauges failed at the USGS stations during the validation event. If the gauge was 'taken out' when the ice front passed, then the results suggest that the model is doing a good job of simulating the timing of the ice front at the USGS gauges for both the calibration and validation events. The timing of the water level rise is not well captured at ESS45 in either the calibration or the validation event. The model is late in predicting the rise for the calibration event but predicts it early for the validation event. The cause of poor performance at this station is unclear; however, it is located immediately upstream of a two mile reach of the river containing mid-channel islands. These islands may be creating two-

Table 2
Simulated and observed values for ice surveys.

	Station and date				
	ESS40	ESS40	ESS45	ESS50	ESS55
	29-Jan-13	26-Jan-14	24-Jan-14	23-Jan-14	25-Jan-14
Average observed solid ice thickness, t_i (m)	1.15	0.75	0.67	0.55	0.62
Maximum observed solid ice thickness, t_i (m)	1.63	1.09	1.13	1.14	0.92
Simulated solid ice thickness, t_i (ft)	1.20	1.02	0.86	0.92	1.04
Observed solid ice cross sectional area, A_{si} (m^2)	170	103	96	63	59
Simulated solid ice cross sectional area, A_{si} (m^2)	169	142	118	56	69
Average observed frazil slush thickness, t_{fs} (m)	1.04	1.78	1.06	2.31	1.71
Maximum observed frazil slush thickness, t_{fs} (m)	2.31	3.53	2.25	5.71	3.26
Simulated frazil slush thickness, t_{fs} (m)	0.90	0.93	2.33	4.28	1.23
Observed frazil slush cross sectional area, A_{fs} (m^2)	153	245	152	262	164
Simulated frazil slush cross sectional area, A_{fs} (m^2)	127	129	319	261	82
Observed width, B_o (m)	148	137	143	114	96
Simulated width, B_o (m)	141	138	137	61	66
Observed flow, Q_w (m^3/s)	52.4	74.0	71.9	69.6	63.6
Simulated flow, Q_w (m^3/s)	73.0	76.5	69.4	66.6	66.6
Observed water level, H (m, a.s.l.)	118.34	118.24	143.34	161.53	256.87
Simulated water level, H (m,a.s.l.)	118.46	118.33	143.86	162.22	256.54

dimensional forces on the water and ice that impacting the ice cover progression through this reach and therefore the arrival time of the ice front at ESS45. Although the timing is off, the model has predicted the magnitude of the water level rise quite well.

Parameters for the under-cover transport follow those suggested by Shen and Wang (1995). Although no data were available to directly calibrate this process, winter ice thickness measurements indicated the presence of significant frazil slush under the solid ice cover, confirming the importance of under-cover transport in the Susitna River's ice regime. Data from winter ice surveys were provided for a few selected cross sections during the freeze-up period. This survey data included bed elevation, top and bottom of frazil slush layer, top and bottom of solid ice layer, water level and flow at the time of survey. This information was used to calculate the cross sectional area of the frazil slush and solid ice layers for the surveys. Average ice thicknesses were calculated from the areas by dividing by the width of the channel at the time of survey. Simulated and observed values at the time of the surveys are presented in Table 2.

Generally the model did a good job of simulating solid ice thickness and cross sectional area. For the most part, the simulated values are between the average and maximum observed thicknesses. The model did not perform as well in simulating the frazil slush. Only at ESS50 were the frazil slush thickness and cross section area in agreement with the observed values. At the other stations, the model either over or underestimated the amount of ice. But considering the temporal nature of undercover ice transport and the 1D approach used to simulate this complex process, the results are reasonable. The simulated flows agree very well with observed ones except on January 29, 2013. On this date, the flow at USGS 15292000 (upstream of ESS40) is reported ranging from 64.1 to 64.3 m^3/s. The simulated flows at USGS 15292000 on this date range from 63.3 to 64.4 m^3/s. Since the model and observed flows are in agreement at the USGS station, the discrepancy at ESS40 is possibly due to survey error. However, it is possible that at the USGS stations, which were used to create the model inflows, flows are not being reported correctly since gauge rating curves do not normally account for the effects of an ice cover. But since all other simulated and observed flows in Table 2 agree so well, it is more likely that the lack of agreement for the 2013 survey is attributable to survey error.

4. Conclusions and recommendations

This paper presents new development of the University of Alberta's comprehensive river ice process model, *River1D*. This public-domain model has been enhanced to include the ability to simulate natural channel geometry, water supercooling, anchor ice formation and release, border ice formation, under-cover transport of frazil, and ice cover progression based on leading edge stability criteria. *River1D* is the first public-domain model to include supercooling and anchor ice evolution. An unprecedentedly comprehensive calibration and validation of the model were conducted with data of the Susitna River, including water levels, flows, water temperatures, surface ice concentrations, border ice widths, ice cover progression rates, and ice thicknesses. Favourable agreements between the modelled and observed data demonstrate the ability of the newly enhanced model for simulating the freeze-up process on this complex natural river. The new natural channel capabilities facilitated good simulation of water levels in both open water and ice covered conditions compared to the observed levels. The new border ice component was able to capture the variability in the observed border ice widths. An additional term, based on a degree-day approach, has been included in the border ice model which provides the user with additional means to calibrate the border ice growth and/or a simpler border ice model that only requires calibration of a single parameter. The new supercooling capabilities allowed for the simulation of anchor ice which, as observations indicate, is an important process on the Susitna River. The presence of significant frazil slush under the solid ice cover confirmed the importance of under-cover transport of frazil in the Susitna River's ice regime and the need to include this process in the simulations. Future developments to *River1D* ice process model are recommended to include the capability to simulate multiple bridging locations and a means of evaluating the stability of the ice cover once it has formed. Lastly, detailed data describing anchor ice evolution and under-cover transport and accumulation are really needed in order to properly evaluate these model components.

Acknowledgement

This research was funded through the Alaska Energy Authority and the Natural Sciences and Engineering Research Council of Canada. Their support is gratefully acknowledged. The data used for calibrating and validating the model were provided by HDR Alaska Inc., and this collaboration is also gratefully acknowledged, with particular thanks to Jon Zufelt for his support and assistance with this research.

List of symbols

A	Cross sectional area to the water surface
A_{an}	Cross sectional area of anchor ice
A_b	Cross sectional area of border ice
A_{fs}	Cross sectional area of the frazil slush layer
A_i	Cross sectional area of surface ice including border ice and under-cover moving frazil
A_{si}	Cross sectional area of the solid ice layer
A_{ui}	Cross sectional area of under-cover moving frazil layer
A_w	Cross sectional area of water under and through the ice
a	Border ice equation coefficient
B_b	Border ice width from a given bank
B_o	Width of open water between border ice at a cross section
B_{bl}	Width of border ice at the left bank
B_{br}	Width of border ice at the right bank
B_{btotal}	Total width of border ice at a cross section
B_{ws}	Total width of the channel at the water surface for main channel excluding overbank flow
b	Border ice equation coefficient
C_{an}	Fraction of bed covered by anchor ice
C_i	Surface ice concentration
C_f	Volumetric concentration of suspended frazil
C_{fo}	Frazil seeding concentration
C_p	Specific heat of water
D	Mean hydraulic depth of water and ice
D_{wi}	Longitudinal dispersion coefficient for the ice-water mixture
D_w	Mean hydraulic depth of water
D_{wl}	Local water depth at the edge of border ice
D_{si}	Longitudinal dispersion coefficient for the surface ice
d	Border ice equation coefficient
d_e	Typical frazil particle radius
d_f	Average diameter of frazil granules in under-cover transport layer
d_s	Bed material average diameter
e	Border ice equation coefficient
e_{wi}	Thermal energy of the water and the suspended frazil (ice-water mixture)
f_1	Conditional constant in solid ice layer transport equation
F	Frazil particle shape factor
F_r	Froude number
F_{r_jux}	Maximum Froude number for juxtaposition
F_{r_max}	Maximum Froude number for ice cover advancement
g	Gravitational acceleration
H	Water surface elevation above a specified datum
h_{wa}	Heat transfer coefficient between water and air
K_i	Thermal conductivity of ice
L	Length of ice cover between computational nodes
L_i	Latent heat of ice
N_u^f	Nusselt number for typical suspended frazil particle
n_b	Manning's roughness coefficient for the bed
n_c	Composite Manning's roughness coefficient
n_i	Manning's roughness coefficient for the ice
P_b	Bed-affected wetted perimeters of the channel
P_i	Ice-affected wetted perimeters of the channel
p_a	Porosity of anchor ice
p_c	Space between ice floes in newly formed ice cover
p_f	Frazil slush porosity
Q_w	Discharge of water under and through the ice
Q_{uit}	Total under-cover ice discharge
Q_{uic}	Ice transport capacity
r_o	Typical frazil particle radius
S_f	Boundary friction slope
S_{ui}	Source term representing exchange between moving and stationary frazil layers
T	Total width of the channel at the water surface
T_w	Average water temperature in the cross section
t	Time variable
Δt	Simulation time step
t_{an}	Anchor ice thickness
t_b	Border ice thickness
t_{fs}	Frazil slush layer thickness
t_f'	New frazil pan thickness
t_{le}	Thickness of ice at the leading edge
t_{si}	Solid ice layer thickness
t'_{si}	Initial ice thickness of newly formed solid ice between stationary ice pans
t_{ui}	Thickness of under-cover moving frazil layer
U_{cr}	Maximum velocity for dynamic border ice growth
U_i	Ice velocity
U_{i_re}	The ice velocity threshold criteria for re-entrainment
U_{ui}	Velocity of under-cover moving frazil layer
U_w	Average water velocity in the cross section
U_{wl}	Local water velocity at the edge of border ice
X_i	Ice front location
x	Streamwise space variable
α_{wi}	Coefficient of turbulent heat exchange
β	Momentum flux correction coefficient
β_{re}	Rate of surface ice re-entrainment
γ	Frazil accretion rate
ε_{wi}	Ice water mixture longitudinal dispersion parameter
ε_{si}	Surface ice longitudinal dispersion parameter
η	Rate of frazil rise
Θ_c	Critical flow strength
μ	Composite jam stress parameter
ρ_i	Density of ice
ρ_w	Density of water
ρ_s	Density of bed material
τ_c	Ice cohesion
Φ_{ia}	Net rate of heat exchange between water and air through the floating ice layer
Φ_{fw}	Net rate of heat exchange per unit surface area between frazil particles and water
Φ_{wa}	Net rate of heat exchange between water and air
Φ_{wi}	Net rate of heat exchange between water and ice
Φ_s	Net incoming solar radiation

References

Andrishak, R., Hicks, F.E., 2005. Impact of climate change on the Peace River thermal ice regime. In: CGU HS Committee on River Ice Processes and the Environment Proc., 13th Workshop on Hydraulics of Ice Covered Rivers, pp. 21–40 September 15–16, 2005, Hanover, NH.

Andrishak, R., Hicks, F., 2008. Simulating the effects of climate change on the ice regime of the Peace River. Can. J. Civ. Eng. 35, 461–472.

Ashton, G.D., 1973. Heat transfer to river ice covers. In: Proceedings of the 30th Eastern Snow Conference, Amherst, Mass., 8–9 February 1973. Eastern Snow Conference, Monmouth, Maine, pp. 125–135.

Ashton, G.D. (Ed.), 1986. River and Lake Ice Engineering. Water Resources Publications, Littleton, Colorado (485 pp.).

Beltaos, S., 2013. Chapter 7: Freezeup Jamming and Formation of Ice Cover. In: Beltaos, S. (Ed.), River Ice Formation. CGU HS Committee on River Ice Processes and the Environment, pp. 181–255.

Beltaos, S., Prowse, T., 2001. Climate impacts on extreme ice-jam events in Canadian rivers. Hydrol. Sci. J. 46 (1), 157–181.

Brooks, A.N., Hughes, T.J.R., 1982. Streamline upwind petrov-galerkin formulations for convection dominated flows with particular emphasis on the incompressible navier-stokes equations. Comput. Methods Appl. Mech. Eng. 32 (1–3), 199–259.

Brown, R.S., Mackay, W.C., 1995. Fall and winter movements and habitat use by cut-throat trout in the Ram River, Alberta. Trans. Am. Fish. Soc. 124, 873–885.

Brown, R.S., Power, G., Beltaos, S., Beddow, T.A., 2000. Effects of hanging ice dams on winter movements and swimming activity of fish. J. Fish Biol. 57, 1150–1159.

Calkins, D.J., 1984. Instream Ice Calibration of Computer Model. Alaska Power Authority Document No. 1122. (111 pp).

Clark, S., 2013. Chapter 3: Border and Skim Ice. In: Beltaos, S. (Ed.), River Ice Formation. CGU HS Committee on River Ice Processes and the Environment, pp. 77–106.

Daly, S.F., 1991. Frazil ice blockage of intake trash racks. In: CRREL Technical Digest 91–1. Army Corps of Engineers Cold Regions Research and Engineering Laboratory, Hanover, New Hampshire (12 pp.).

Fread, D.L., 1988. The NWS DAMBRK Model: Theoretical Background/User Documentation. Office of Hydrology, National Weather Service (NWS), Maryland, U.S.A.

Fread, D.L., Jin, M., Lewis, J.M., 1996. An LPI Numerical Solution for Unsteady Mixed Flow Simulation, North American Water Congress. American Society of Civil Engineers, Anaheim, CA, pp. 1–7 June 22–28, 1996.

Girling, W.C., Groeneveld, J., 1999. Anchor Ice Formation Below Limestone Generating Station. In: CGU HS Committee on River Ice Processes and the Environment Proc., 10th Workshop on Hydraulics of Ice Covered Rivers, pp. 160–173 Winnipeg, Manitoba, Canada.

Haresign, M., Toews, J.S., Clark, S., 2011. Comparative testing of border ice growth prediction models. In: CGU HS Committee on River Ice Processes and the Environment Proc., 16th Workshop on River Ice, pp. 400–412 September 18–22, 2011, Winnipeg, MB.

HDR, Alaska Inc., 2014. Ice Processes in the Susitna River Study, Study Plan Section 7.6, Initial Study Report. Prepared for Alaska Energy Authority. (51 pp.).

Hicks, F.E., Steffler, P.M., 1990. Finite element modeling of open channel now. In: Water Resources Engineering Report No. 90–6. Department of Civil Engineering, University of Alberta, Edmonton, AB (356 pp).

Hicks, F.E., Steffler, P.M., 1992. A characteristic dissipative galerkin scheme for open channel flow. ASCE J. Hydraul. Eng. 118, 337–352.

Hutchison, T.K., Hicks, F., 2007. Observations of ice jam release events on the Athabasca River, AB. Can. J. Civ. Eng. 34 (4), 473–484.

Jasek, M., Ghobrial, T., Loewen, M., Hicks, F., 2011. Comparison of CRISSP modeled and SWIPS measured ice concentrations on the Peace River. In: CGU HS Committee on

River Ice Processes and the Environment Proc., 16th Workshop on River Ice, pp. 249–273 September 18–22, 2011, Winnipeg, MB.
Jasek, M., Shen, H.T., Pan, J., Paslawski, K., 2015. Anchor ice waves and their impact on winter ice cover stability. In: 18th CGU-HS Committee on River Ice Processes and the Environment Proc. 18th Workshop on the Hydraulics of Ice Covered Rivers. vol. 2015 Quebec City, Quebec, August 18–20.
Kammerer, J.C., 1990. Largest rivers in the United States: U.S. Geological Surv. Open File Rep. 87-242 (2 pp).
Kerr, D.J., Shen, H.T., Daly, S.F., 2002. Evolution and hydraulic resistance of anchor ice on gravel bed. J. Cold Reg. Sci. Technol. 35 (2), 101–114.
Kovachis, N., 2011. Patterns of river breakup timing and sequencing, Hay River, NWT. M.Sc. Thesis. University of Alberta, Edmonton, Canada.
Lal, A.M. W., Shen, H. T. 1991. A mathematical for river ice processes, J. Hydraul. Eng., ASCE, 117(7): 851–867.
Lindenschmidt, K.E., 2017. RIVICE – a non-proprietary, open-source, One-dimensional river-ice model. Water 9 (5), 314 (1-15).
Malenchak, J., 2011. Numerical Modelling of River Ice Processes on the Lower Nelson River. Ph.D. Thesis. University of Manitoba, Winnipeg, Canada.
Matousek, V., 1984. Types of Ice Run and Conditions for their Formation. In: Proceedings of 7th IAHR International Symposium on Ice. vol. 1. pp. 315–327 Hamburg, Germany.
Michel, B., Marcotte, N., Fonseca, F., Rivard, G., 1982. Formation of border ice in the Ste. Anne River. In: Proceedings of the Workshop on Hydraulics of Ice-Covered Rivers. University of Alberta, Edmonton, Alberta, Canada, pp. 38–61.
Nash, J.E., Sutcliffe, J.V., 1970. River flow forecasting through conceptual models, part 1—a discussion of principles. J. Hydrol. 10 (3), 282–290.
Nezhikhovskiy, R.A., 1964. Coefficients of roughness of bottom surface on slush-ice cover. In: Soviet Hydrology. American Geophysical Union, Washington, pp. 127–150 Selected Papers 2.
Pariset, E., Hausser, R., 1961. Formation and evolution of ice covers on rivers. Trans. Eng. Inst. Can. 5, 41–49.
Pariset, E., Hausser, R., Gagnon, A., 1966. Formation of ice covers and ice jams in rivers. ASCE J. Hydraul. Div. 92 (HY6), 1–24.
She, Y., Hicks, F., Steffler, P., Healy, D., 2009. Constitutive Model for internal resistance of moving Ice accumulations and eulerian implementation for river ice jam formation. J. Cold Reg. Sci. Technol. 45, 137–147.
Shen, H.T., 2006. A one-dimensional comprehensive river ice model. In: Proceedings of the 18th IAHR International Symposium on Ice, Sapporo, Japan, pp. 61–68.
Shen, H.T., 2010. Mathematical modeling of river ice processes. Cold Reg. Sci. Technol. 62, 3–13.
Shen, H.T., 2016. Chapter 9: River ice processes. In: Wang, L.K., Yang, C.T., Wang, M.-H.S. (Eds.), Advances in Water Resources Management. Springer International Publishing, Switzerland, pp. 483–530.
Shen, H.T., Wang, D.S., 1995. Under cover transport and accumulation of frazil granules. J. Hydraul. Eng. 121 (2), 184–194 ASCE.
Shen, H.T., Wang, D.S., Lal, A.M.W., 1995. Numerical simulation of river ice processes. J. Cold Reg. Eng. ASCE 9, 107–118.
Tetra Tech, Ice, 2013. Initial Geomorphic Reach Delineation and characterization, middle and lower susitna river segments (FERC no. 14241). In: Prepared for Alaska Energy Authority, February 2013, (24 pp.).
Theriault, I., Sucet, J.-P., Taha, W., 2010. Validation of the Mike-Ice model simulating river flows in presence of ice and forecast of changes to the ice regime of the Romaine River due to hydroelectric project. In: Proceedings of the 20th IAHR International Symposium on Ice, Lahti, Finland.
Timalsina, N., Charmasson, J., Alfredsen, K.T., 2013. Simulation of the ice regime in a Norwegian regulated river. Cold Reg. Sci. Technol. 94, 61–73.
Tsang, G., 1970. Change of velocity distribution in a Cross-section of a Freezing River and the effect of frazil ice loading on velocity distribution. In: Proceedings of the 1st International Symposium on Ice. International Association of Hydro-Environment Engineering and Research, Reykjavik, Iceland, pp. 1–11.
Uzuner, M.S., 1975. The composite roughness of ice covered streams. J. Hydraul. Res. 13, 79–102.
Uzuner, M.S., Kennedy, J.F., 1976. Theoretical model of river ice jams. ASCE J. Hydraul. Div. 102 (HY9), 1365–1383.
Wang, D.S., Shen, H.T., Crissman, R.D., 1995. Simulation and analysis of upper Niagara River ice-jam conditions. J. Cold Reg. Eng. 9 (3), 119–134.